Titre: Title:	Material extrusion additive manufacturing of multifunctional sandwich panels with load-bearing and acoustic capabilities for aerospace applications
Auteurs: Authors:	Juliette Pierre, Filippo Iervolino, Rouhollah D. Farahani, Nicola Piccirelli, Martin Lévesque, & Daniel Therriault
Date:	2023
Type:	Article de revue / Article
Référence: Citation:	Pierre, J., Iervolino, F., Farahani, R. D., Piccirelli, N., Lévesque, M., & Therriault, D. (2023). Material extrusion additive manufacturing of multifunctional sandwich panels with load-bearing and acoustic capabilities for aerospace applications. Additive Manufacturing, 61, 103344 (10 pages). https://doi.org/10.1016/j.addma.2022.103344

Titre de la revue: Journal Title:	Additive Manufacturing (vol. 61)
Maison d'édition: Publisher:	Elsevier
URL officiel: Official URL:	https://doi.org/10.1016/j.addma.2022.103344
Mention légale: Legal notice:	

Material extrusion additive manufacturing of multifunctional sandwich panels with load-bearing and acoustic capabilities for aerospace applications

Juliette Pierre[1*], Filippo Iervolino[1], Rouhollah D. Farahani[1], Nicola Piccirelli[2], Martin Lévesque[1] and Daniel Therriault[1]

[1]Laboratory for Multiscale Mechanics (LM[2]), Department of Mechanical Engineering, Research Center for High Performance Polymer and Composite Systems (CREPEC), Polytechnique Montréal, Montréal, Canada

[2]Safran Composites, Itteville, France

E-mail: juliette.pierre@polymtl.ca

Abstract

Reducing the noise produced by airplane engines is a significant challenge for the aerospace industry. In the present work, we investigate the design and fabrication of an acoustic sandwich panel featuring wider sound-absorbing performance compared to the currently employed technologies (e.g., perforated honeycomb cell sandwich panels). The use of material extrusion additive manufacturing (MEAM) enables us to create panels in one manufacturing step with complex geometry. The developed multifunctional (i.e., mechanical and acoustic) sandwich panel, which is based on the combination of five Helmholtz resonators, demonstrates an absorption spectrum over 517 Hz when measured with an impedance tube. The developed acoustic design, named Trapezoidal Compact (TC) sandwich, has an acoustic spectrum with more than 90% of absorption, comprised between 643 Hz and 1160 Hz. Three-point bending tests revealed that the stiffness of the sandwich panels with the TC geometry is up to ~10% higher than those of the panels with a standard hexagonal honeycomb (HC) structure, additively manufactured with the same mass and wall thickness. The design developed in this work will contribute to the improvement of additive manufacturing process of multifunctional structures for aerospace applications.

Abbreviations

AM, additive manufacturing; FFF, fused filament fabrication; HC, hexagonal honeycomb; HR, Helmholtz resonator; MEAM, material extrusion additive manufacturing; PLA, polylactic acid; TC, trapezoidal compact.

Keywords

Additive manufacturing, FFF, Helmholtz resonator, multifunctional structures, sandwich panel

1. Introduction

Along with weight reduction, noise pollution has been targeted as a crucial improvement factor for the future of aviation by international organizations [1]. Indeed, airplanes are among the noisiest nuisances people have to deal with in their everyday lives [2]. The noise emitted by airplanes can be divided in two categories: emissions by airframes [3] and emissions by engines. In this study, we focus on the latter, which represents the most important noise source, spreading over a few thousand Hertz [4]. Different types of structures have already been studied to decrease this pollution. For example, porous structures such as micro scaffolds [5] and micro lattices [6] have demonstrated properties to reduce engine noise down to 90% in the frequency range of 2000-3000Hz. However, between 500 Hz and 1200 Hz, no solution combining an absorption band of several hundred of Hertz and an absorption above 90% has been found yet. Micro perforated plates and Helmholtz resonators (HRs) have demonstrated >90% of absorption between 500-1500 Hz but the absorption range is usually very narrow (i.e., ~100-200Hz wide) [7][8]. An HR is composed of a cavity with a volume V_c, a cylindrical neck with a length L_n and a diameter D_n. These parameters determine the natural frequency of its resonating chamber [9]. The natural frequency of the resonator f_r, can be found by:

$$f_{\mathrm{r}} = \frac{c}{2\pi}\sqrt{\pi {D_n}^2 / V_c L_n} \ , \quad (1)$$

where c is the speed of sound in the medium of interest.

The shape of the cavity of the resonator does not intervene in Equation (1). It does not impact the natural frequency as long as the cavity length is longer than the neck diameter and that the width and depth of the cavity have the same order of magnitude [10].

HRs have already been included in sound-absorbing acoustic sandwich panels to reduce the noise emitted by aircraft engines [11]. They are usually placed on fan cases, which are the cylindrical structures around the engines. These sandwich panels are typically constituted of a hexagonal honeycomb core and two skins. Although a honeycomb pattern is repeatable and relatively easy to produce at a large scale through folding [12], the fabrication of a honeycomb sandwich panel requires additional steps such as manufacturing of the face sheets and the core separately and their assembly [13].The upper skin must also be perforated before assembly to add the HRs sound-absorbing functionality to the empty cells located in the core of the sandwich structure [14]. It is then impossible to create a panel in one step of fabrication with conventional folding methods since the core and the face sheets are produced in two very distinct ways. In addition, with this method, every cavity has the same dimensions and geometry. With a hexagonal honeycomb configuration with identical cell sizes and skin holes diameters, all the HRs absorb only one frequency of noise. However, combining different HRs can widen the absorption peak, up to a few hundred Hertz [14]. A common technique is to stack one panel on another panel, each with a different perforation size [15]. The main drawback of this stacking method is the increase of thickness and weight of the panel, while still absorbing a relatively narrow acoustic spectrum. However, creating a greater variety of cavities on one layer of a panel would be less repeatable than regular hexagonal honeycombs and therefore more difficult to manufacture through folding or any conventional type of fabrication.

Material extrusion additive manufacturing (MEAM), and more precisely Fused Filament Fabrication (FFF), consists in the layer-by-layer deposition of a hot extruded thermoplastic-based filament through a nozzle of a precise diameter [16]. Many types of thermoplastic (neat or reinforced) filaments can be used [17] [18], such as Polylactic Acid (PLA) [19], Acrylonitrile Butadiene Styrene (ABS) [20], carbon reinforced Nylon [21] or Polyetherimide (PEI) [22]. Using the FFF process, sandwich panels can be printed in a single step of fabrication [23]. Sandwich panels are very frequently used for aerospace structures due to their good mechanical properties in bending [24]. Several sandwich panels have already been crafted with AM ~~for their mechanical properties in bending~~. For example, different sandwich panels with truss-like lattices core have been printed with PLA and tested under 3-point bending [25]. Additively manufactured sandwich panels made of ULTEM9085 (PEI) have also been tested under 4-point bending: a degradation of the mechanical bending properties has been observed with the thinning of the walls of the panel [26]. A 60 mm-thick 3D-printed panel combining 4 HRs and 8 double HRs has achieved a 900Hz wide absorption range (i.e., between 450 Hz–1360 Hz) due to the creation of double HR through AM but has not been submitted to mechanical testing; concluding that AM is an alternative method to manufacture the panels, featuring complex core designs with several combined HR geometries for optimal sound-absorbing performance [27]. A perforated and corrugated honeycomb sandwich panel has been simulated for its acoustic and load-bearing capabilities but has not been manufactured [28].

Table 1 sums up the several additively manufactured sandwich panels with bending mechanical or acoustic properties cited above. The reported FFF printed panels have been designed for their bending mechanical properties or their sound-absorbing functionality (i.e., acoustic performance). However, to the best of the authors' knowledge, none of the works

have explored the manufacturing of the two functionalities for sandwich panels, i.e., acoustic performance and enhanced flexural properties, simultaneously.

Functionality	Type the panel	Material	Main	Author
Acoustic	Simulation	-	Perforation on the upper skin and the core; 500-1000 Hz absorption range above 75% (mechanical performances in bending due to the honeycomb core)	Tang et al. [28]
			Combination of 9 HR; 600-1100 Hz absorption range above 90%	Peng et al. [14]
	FFF	PLA	Combination of 4 HR and 4 double HR; 450-1350 Hz absorption range above 80%	Liu et al. [26]
Mechanical	FFF for the core	PLA	Bending test = mechanical properties depend on the shape of the core	Azzouz et al. [25]
	FFF for the whole panel	PLA	Bending = printing direction and shape of the core impact mechanical performances	Sarvestrani et al. [23]
		PEI	Bending = the skin/core interface quality decreases with the wall thickness decrease	Bagsik et al. [26]

Table 1 Summary of the main additively manufactured sandwich panels that are optimized either for their bending or their acoustic performances.

In this work, we investigated a design for the geometry of sandwich panels featuring a wide range sound-absorbing acoustic performance at low frequencies while maintaining flexural mechanical properties, when compared to 3D printed honeycomb sandwich panels. Our designed sandwich panel contains a combination of several HRs of different volumes in its core. In addition to its acoustic performance, the flexural mechanical performance of the sandwich panel under 3-point bending was compared to that of a 3D printed honeycomb sandwich panel, also in PLA, to verify that the geometry used would not adversely affect the mechanical performance of the panel in bending.

2. Materials and methods

2.1. Geometrical design of the acoustic sandwich panel

A structure named Trapezoidal Compact (TC) containing 5 HRs was designed using CATIA V5, as shown in Figure 1a. The 5-HR unit was chosen as a square to create a repeatable pattern for a sandwich panel, as shown in Figure 1b. The thickness of the core and the skins was fixed to 30 mm and 3 mm, respectively.

The dimensions of the holes were computed with Equation (1) to obtain an absorption peak every ≈ 125 Hz, to obtain peaks close enough to create a continuous spectrum with an absorption above 90% [14][27]. Acoustic specimens were adapted from the square 5-HR unit using CATIA V5 to cylindrical specimens with a diameter of 30 mm to fit in the available acoustic test equipment. The thickness of the walls of the acoustic specimens was set at 0.8 mm. The pattern was repeated twice in the width direction and four times in the length direction to create the sandwich panel having dimensions of 205 mm × 76 mm × 36 mm, so that it complied with the requirements of the ASTM D7250 standard for bending testing, as shown in Figure 1d.

A hexagonal honeycomb (HC) sandwich panel was also created using CATIA V5 to compare the mechanical and acoustic performance of the TC panel. The HC panel had the same density, the same overall dimensions, and the same wall thickness as the TC panel. The volume of its cavities, all identical, was not chosen but dictated by the density of the panel. An acoustic specimen was created for the HC geometry. It contained only one honeycomb extracted from the sandwich panel to test the absorption of one HR at a time.

For each TC and HC configuration, two different designs were created: one with 0.8 mm thick walls and one with 0.4 mm thick walls, to relate the stiffness and maximum supported load against the weight of the panels. The holes of the upper skin were removed for the mechanical

tests so that the two types of panels had similar skins and since we are mainly interested in comparing the flexural performance of the two different types of cores.

2.2. 3D printing of the acoustic specimens and the sandwich panels

The acoustic specimens were printed using a 0.4 mm FFF nozzle fed by PLA filaments so that two filaments printed side by side created a ≈ 0.8 mm wall thickness. In addition to the acoustic specimens, three sets of sandwich panels were printed. Each set was constituted of a TC sandwich panel and of its HC counterpart, with the same overall size and weight. A 0.4 mm nozzle was used to print one set of 0.4 mm thick walls and one pair of 0.8 mm thick walls by extruding two 0.4 mm filaments. A 0.8 mm nozzle was used to print the last set of 0.8 mm thick walls. Table 2 summarizes the different types of sandwich panels printed. The terminology of the different panels is defined by [type of geometry][identification of the size of the nozzle]×[number of filaments to create the thickness of the wall]. For example, the nominal thickness of the wall of TC4×1 is 0.4 mm and that of HC4×2 is 0.8 mm.

	Type of samples			
	TC	HC	Wall thickness (mm)	Nozzle diameter (mm)
Name of samples	TC4×1	HC4×1	0.4	0.4
	TC4×2	HC4×2	0.8	0.4
	TC8×1	HC8×1		0.8

Table 2 Geometrical specification of each configuration of the printed panels.

The specimens were printed using a Raise3D Pro2 3D printer and PLA Raise 3D premium material. Simplify3D was the software used to slice the parts to print. The printing and the bed temperatures were 210°C and 60°C, respectively. The printing speed was 60 mm/s, the extrusion multiplier was 0.9 and the extrusion width was set to 0.4 mm for the nozzle having a diameter of 0.4mm and to 0.8 mm for the nozzle having a nozzle of 0.8 mm. The layer thickness was set to 0.2 mm for all panels. The filling was 100% and one outline perimeter was printed. The G-code was generated from Simplify3D.

2.3. Printed part inspection

A reference CAD model of the targeted diameter holes was created using CATIA V5 to verify the accuracy and repeatability of the printing process. The reference CAD model had a rectangular shape of 10 mm by 41.5 mm featuring 6 holes of different diameters (1 mm, 1.5 mm, 2 mm, 2.5 mm, 3 mm and 3.5 mm). This CAD model was printed 5 times with a nozzle of 0.4 mm and a nozzle of 0.8 mm. The printing parameters used to print the sandwich panels were the same used here. A verification of the dimensions was made with an optical microscope. Two measures per holes are used to determine the diameter of one specific hole. The printing time of each panel was recorded, and all printed panels were weighted with a scale precise to 0.1 gram.

The printing quality was also assessed through the use of an Olympus SZX12 stereo microscope. Pieces of the different panels were analyzed under the optical microscope to assess the quantity of defects on the printed surfaces. Pictures and measurements were made using the software Image-Pro Plus 7.0.

2.4.Acoustic testing in an impedance tube

The acoustic specimens were tested using an impedance tube having a diameter of 3 cm equipped with two microphones. The tests were conducted in accordance with ASTM E1050 standard. The specimens were placed in a tube and frequencies between 80 Hz and 6500 Hz were emitted at the entrance by the speaker. The two microphones measured the sound absorbed by the specimen. The software INTAC was used to launch the test and record the data. A piece of tape was placed on the holes that were not tested to obstruct them, when testing the acoustic performance of a specific HR contained in a 5HR cell.

2.5. Three-point bending testing

Three point bending testing was conducted using an MTS INSIGHT (Eden Prairie, USA) machine equipped with a 50 kN load cell. The span length was 15.6 cm and the crosshead speed was 5 mm/min. Three specimens for each panel configuration were tested. The effect of the wall thickness, of the core geometry and of the filament size for three-point bending mechanical properties were investigated. The stiffness of each type of panel was computed through a linear regression of the load displacement curves. For each type of panels, 160 points of measure are chosen : between 0.75 mm and 2.10 mm of displacement for the panels with a core thickness of 0.8 mm and between 0.4 mm and 1.75 mm of displacement for the panels with a core thickness of 0.4 mm. The R^2 coefficient was found higher than 0.998.

3. Results and discussion

3.1. Design of sandwich panel

Figure 1 shows the acoustic design of the TC structure as a square cell featuring five HRs which were used to fabricate the cylindrical acoustic testing specimens and the rectangular sandwich panels. The acoustic unit was composed of four trapezoidal hollow shapes and confined by an external wall that created the fifth larger cavity. The perforated skin with 5 holes on top behaved as the neck of the HRs. Figure 1a shows a schematic of one trapezoidal cavity topped by a perforated wall. In Figure 1b, the 4 trapezoidal cavities are identical but alternately turned upside down. Fillets of 2 mm on both sides of each trapezoidal shape were added to improve the adhesion between the core and the skins of the panels. The 3 mm-thick skins were added above and below the four trapezoidal cavities, and two walls were added on the sides to enclose the fifth cavity. Figure 1c shows a unit of the TC panel consisting of the 5 HRs, printed without the skin and with a 0.4 mm wall thickness. Figure 1d shows the schematic of the sandwich panel obtained after the replication of the 5-HR unit, identified

with dotted lines. Figure 1e represents a TC panel having a length of 12 cm, printed with a 0.4 mm nozzle to achieve a 0.8 mm wall thickness, with the upper skin partially printed to expose the cavities inside. Figure 1f shows a TC acoustic specimen with the perforated skin and Figure 1g shows a similar specimen without its top skin. Figure 1h represents a HC panel, used as a reference to compare with the TC panel.

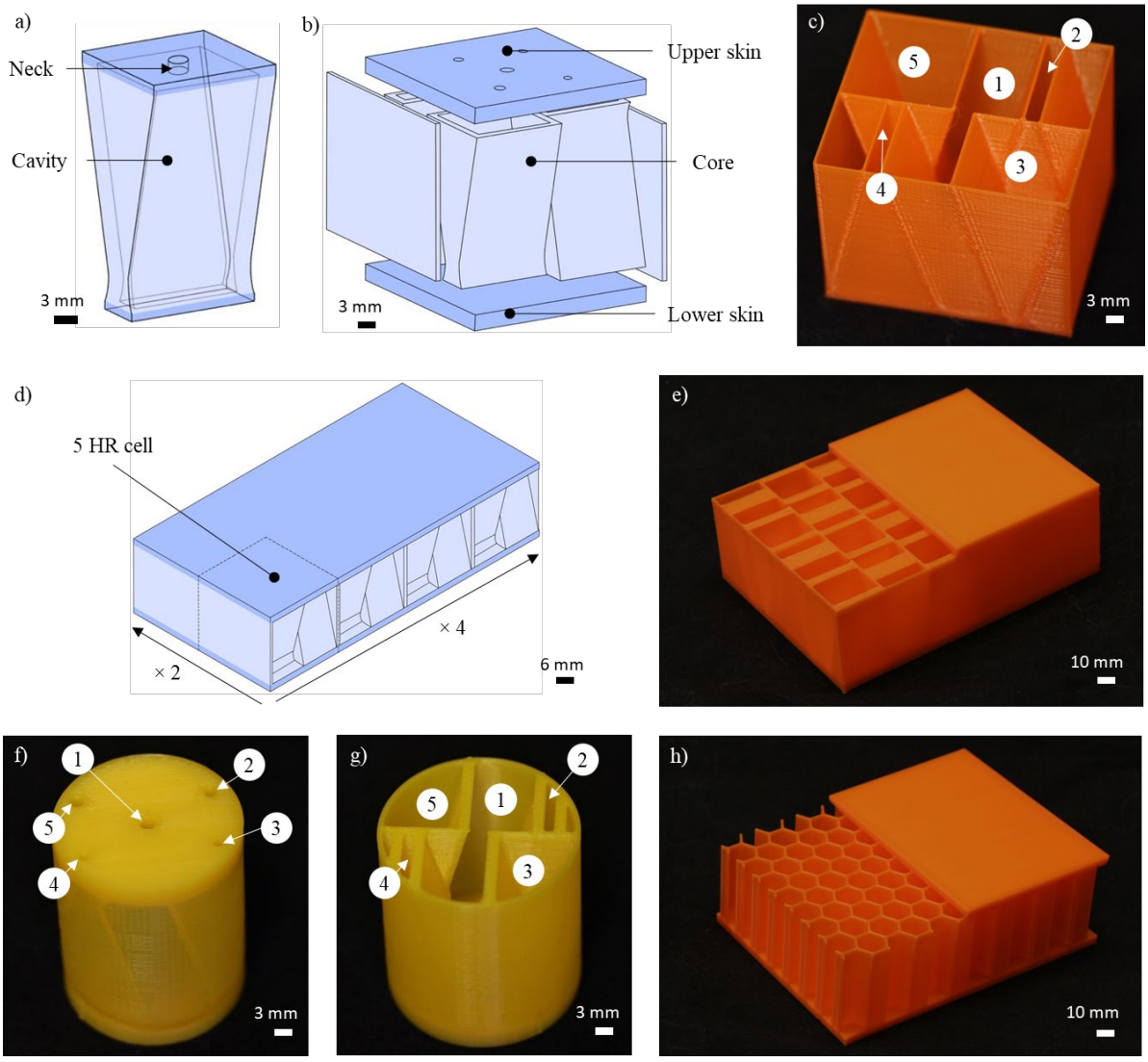

Figure 1 Geometry of the TC acoustic specimen and TC and HC sandwich panels: a) Schematic of one of the hollow trapezoidal shapes acting as a HR, b) Schematic of the 5-HR acoustic cell, constituted of the four hollow trapezoidal shapes and the walls forming a fifth cavity, c) Picture of a cell of 5 HRs without the perforated skin (3D printed with PLA and 0.4 mm thick walls), d) Schematic of a sandwich panel with a highlighted 5-HR cell, e) Picture of a TC sandwich panel; the upper skin is partly removed to display the core with the geometry (3D printed with PLA and 0.8 mm thick walls), f) Picture of an acoustic specimen containing 5-HR cavities with each perforation identified from 1 to 5 with the perforated upper skin (3D printed with PLA and 0.8 mm walls thickness), g) Picture of a similar specimen without the upper skin and each cavity identified from 1 to 5, h) Picture of an HC

sandwich panel; the upper skin is partly removed to display the core with the geometry (3D printed with PLA and 0.8 mm walls thickness).

3.2. Printed parts inspection and improvements

Table 3 compares the diameters of the holes printed with a nozzle having a diameter of 0.4 mm and a nozzle having a diameter of 0.8 mm, and the diameter of the holes of the reference CAD model. The relative difference between the diameter of the holes of the reference CAD model and the measured diameters of the printed holes is also expressed. Figure 3a shows the CAD model. Figure 3b shows a specimen printed with a nozzle having a diameter of 0.4 mm and Figure 3c a specimen printed with a nozzle having a diameter of 0.8 mm. When using a nozzle having a diameter of 0.4 mm, the relative difference between the CAD model and the actual specimen is smaller than 1% for the hole diameters ranging from 1.5 to 3.5 mm. The printed hole with a diameter of 0.86 mm is 14% smaller than the reference CAD model of 1 mm. Using a nozzle having a diameter of 0.8 mm, the diameters ranging from 1.5 mm to 3.5 mm have less than 4% of relative difference with respect to the dimension of the CAD model. The hole of 1 mm of diameter on the CAD model is ~ 24% smaller once printed with a nozzle having a diameter of 0.8 mm. The 95% confidence interval is generally smaller for the holes produced with a nozzle having a diameter of 0.4 mm than for the holes created with the 0.8 mm nozzle. Thus, using a nozzle having a diameter of 0.4 mm provides more accurate and more repeatable holes dimensions than using a nozzle having a diameter of 0.8 mm to print holes having nominal diameters ranging from 1 to 3.5 mm. When looking for the print of a hole with a diameter of 1 mm, the hole in the CAD file should be adjusted with a diameter accounting for the size reduction between the CAD file and the manufacturing of the part (a printed hole will be 86% smaller than in the CAD file with a nozzle having a diameter of 0.4 mm and 77% smaller with a nozzle having a diameter of 0.8 mm).

Targeted hole diameter (mm)	Nozzle size (mm)			
	0.4		0.8	
	Measured hole dia. (mm)	Ratio (%)	Measured hole dia. (mm)	Ratio (%)
1	0.86 (± 0.02)	85.9	0.77 (± 0.01)	77.5
1.5	1.49 (± 0.01)	99.2	1.45 (± 0.05)	96.4
2	2.01 (± 0.02)	100.4	1.92 (± 0.05)	96
2.5	2.50 (± 0.02)	100.1	2.46 (± 0.03)	98.3
3	3.02 (± 0.02)	100.7	2.98 (± 0.02)	99.5
3.5	3.51 (± 0.02)	100.3	3.44 (± 0.03)	98.4

Table 3 Comparison between the dimension of the holes of the CAD model and the printed specimens with a nozzle having a diameter of 0.4 mm and a nozzle having a diameter of 0.8 through optical measurements with the targeted diameter to printed diameter ratio and their 95% confidence interval (five specimens per category, two optical measurements per hole).

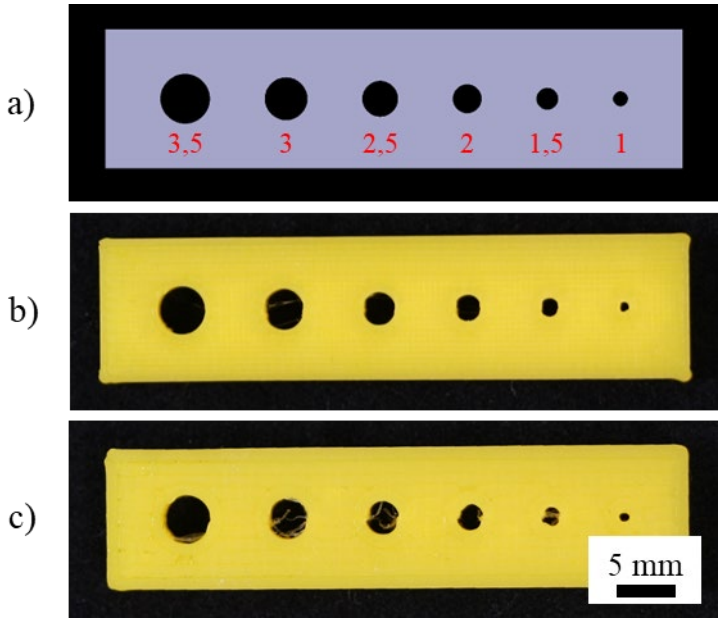

Figure 2 Reference CAD model of the targeted diameter holes and the 3d printed specimens a) Reference CAD model of the targeted diameter holes to compare to the performance of the printed holes, with the diameter of the printed holes indicated in mm b) Specimen printed in PLA with a nozzle having a diameter of 0.4 mm, c) specimen printed in PLA with a nozzle having a diameter of 0.8 mm.

Table 4 compares the different printing times for each type of sandwich panels, along with their weight. Panels printed with a nozzle having a diameter of 0.8 mm are faster to print, as expected. The printing time of panels 04×1 are in between the printing times of panels 08×1 and panels 04×2, which is also expected since the printing time of the skins is the same as for the panels 04×2 and the printing time of the core is about the same as that of the panels 08×1,

since one passage of the nozzle is needed to create a wall. Measurements of the printing time showed that printing one skin with a nozzle having a diameter of 0.4 mm takes 3h30, twice as long as when printing with a nozzle having a diameter of 0.8 mm. The time to print the core is therefore almost the same for all honeycomb panels, suggesting that the travel path generated by Simplify 3D is not optimized for a single extrusion path to print the core wall. In the case of the TC panels, panels with a single extrusion in the core are printed faster than the TC04×2. Printing the TC panels also is faster than printing their HC counterparts, which could be explained by the fact that HC panels have smaller features to print and TC panels encounter less stop and go during a print. The fabrication time, ranging between ~9 hours and ~20 hours, could be decreased by using a high flowrate printing system [29] or Automated Fiber Placement [30] combined to a FFF system. Even nozzles having diameters larger than 0.8 mm could also be used for the skins to improve the manufacturing process. A more optimized travel path could also reduce the manufacturing time of the core.

Panels with a core wall of 0.8 mm have a weight of ~190g and panels with a core wall of 0.4 mm have a weight of ~150g, meaning that TC panels and their benchmark with honeycomb possess the same density, which was required to compare similar panels for the 3-point bending tests.

Type of panels	Printing duration	Average panel weight (g)
TC08×1	9h15	191,2 (± 1.1)
TC04×2	14h00	189.7 (± 0.2)
TC04×1	13h05	153.1 (± 0.6)
HC08×1	15h50	193.8 (± 0.7)
HC04×2	19h50	190.9 (± 0.9)
HC04×1	19h30	153.2 (± 0.1)

Table 4 Comparison of printing time and weight of each type of sandwich panels. Printing times have been rounded to the next 5 minutes to account for the heating time variability. The average panels weights are indicated with their 95% confidence interval (three different specimens per type of panels).

Figure 3a shows a structure printed with a nozzle having a diameter of 0.4 mm with a 2 mm fillet (i) and without fillets (ii). The fillets, of 2 mm of radius, were chosen as the largest fillets before modifying the thickness of the upper skin above the cavities 2 and 4 of Figure 1c. Figure 3b shows the surface quality of a section printed for a visual inspection of a TC8×1 (i) and a TC4×2 (ii) panels. The surface of the section of TC8×1 presents small gaps up to 1 mm long in the direction of deposition of the filament, which is less the case with the section of panel TC4×2. When comparing the two sections, the TC8×1 presents approximately 7 times more defects than the TC4×2. A wall printed with two filaments side by side (TC4x2) has a better printing quality than a wall of the same thickness printed with only one extrusion, when using the same printing speed. However, the printing speed could be reduced to improve the single filament deposition [31]. Indeed, numerous imperfections could decrease the acoustic performance, as the resonator is supposed to be airtight, except for the neck hole [32].

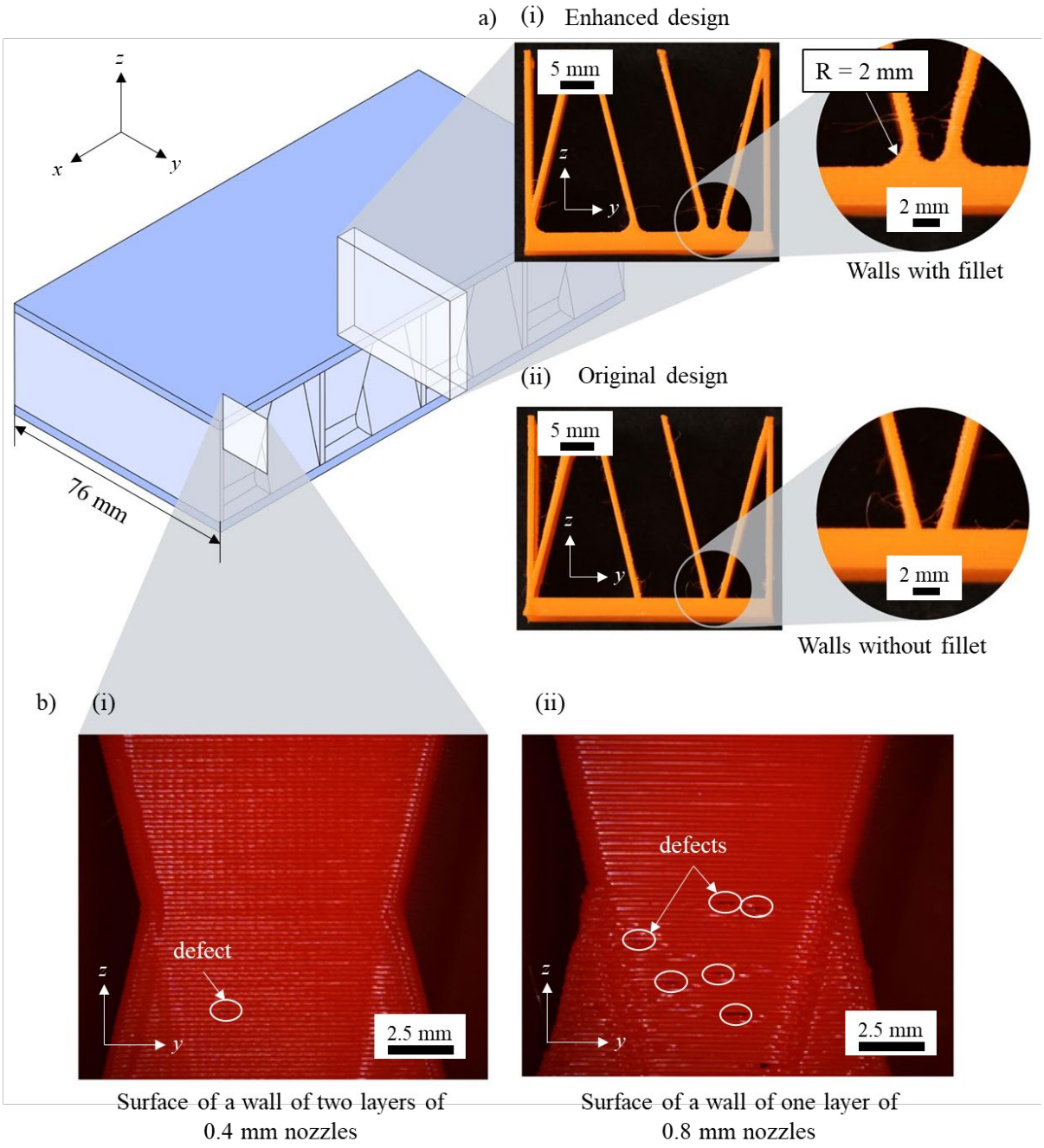

Figure 3 Visual inspection of wall sections of the TC panels, where fillets having a radius of 2 mm and printed with a nozzle having a diameter of 0.4 mm improve the printing quality: a) TC structure printed with and without fillets. b) Details of the surface of printed sections TC4×2 and TC8×1 where the section TC8×1 exhibits more printing defects than the section TC4×2.

3.3.Acoustic performance

Figure 4a shows the schematic of an impedance tube in which the cylindrical specimens were acoustically tested. Figure 4b shows the drawing of the acoustic TC specimens with the five cavities numbered from 1 to 5. Figure 4c shows the absorption curves of each individual

cavity of the TC specimens, when compared to the absorption of the whole multi-resonator (i.e., 5 HRs combined). Five peaks are visible on the general absorption spectrum, corresponding to the five individual absorption peaks for each cavity. As shown in Table 5, these five cavities, when individually tested, yielded the following maximum absorptions frequencies: 789 Hz, 889 Hz, 1012 Hz and 1141 Hz for the four identical cavities, due to their different necks diameters, and 651 Hz for the larger central cavity.

However, as the cavities #1 to #4 have the same volume, the decrease of the neck diameter also results in a decrease of the absorption percentage: holes #4, #3, #2 and #1 have a percentage of absorption of 95% at 1141 Hz, 92% at 1012 Hz, 86% at 889 Hz and 79% at 798 Hz, respectively. It was not possible to obtain a high absorption percentage (>90%) at a frequency lower than ≈950 Hz using the volume of the first four cavities. The main reason seems to be because the hole is too small to allow a satisfactory functioning of the HR, even if Equation (1) is satisfied. Indeed, this result does not happen with the central cavity: even if it absorbs at the lowest frequency of the full spectrum (i.e., 643 Hz), its volume is approximately 3 times larger than one of the four other identical cavities, enabling its neck diameter to be larger than those in the other HRs.

Although the individual absorption of each peak is not always higher than 90%, they interact together well since the absorption between the peaks on the spectrum of the 5HR configuration is always higher than 90%. The absorption starts increasing at a frequency of approximately 500Hz, reaching 98% at 643 Hz, then stays above 90% until 1160 Hz, where it starts to slowly decrease.

Figure 4d displays the absorption of the central cavity and its HC counterparts, whose neck has been designed to absorb at the same frequency. The absorption of the HC acoustic specimen is lower: 70%, when compared to 98%. This result is due to the dimensions of the HC HR. To obtain TC and HC panels with the same density (characteristic chosen for the

mechanical tests), the honeycomb cells had to be small enough to be limited in the reach of lower acoustic frequencies, such as 700 Hz.

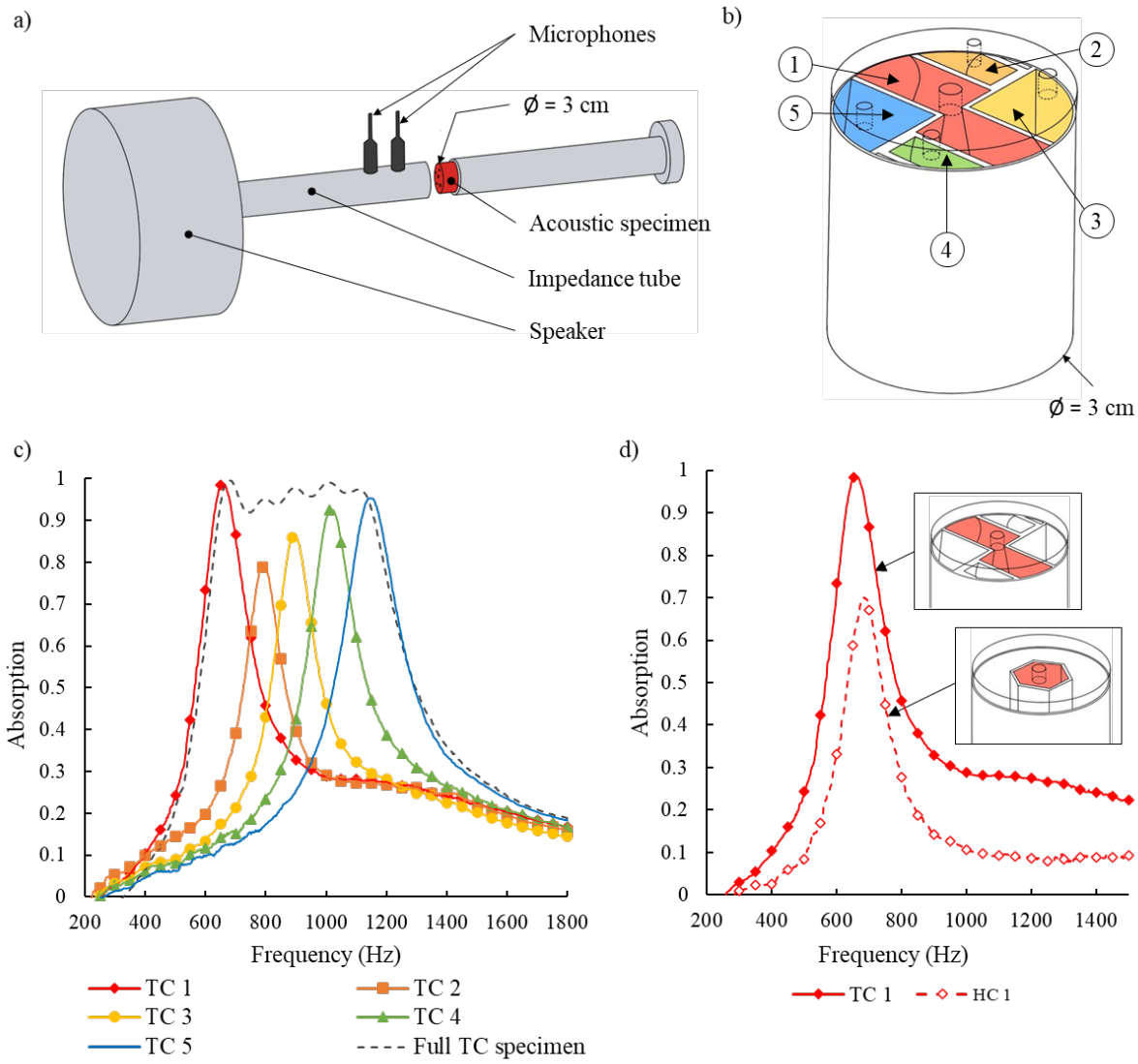

Figure 4 Acoustic absorption of TC specimens and comparison with HC specimens. a) Schematic of an opened impedance tube b) TC acoustic specimen with the 5 acoustic cells identified c) Absorption spectrum of each cavity of TC design independently tested and all cavities tested together on a 200-1800Hz range : the global absorption is above 90% between 643-1160 Hz d) Absorption spectrum of the cavity #1 of the TC design and the absorption obtained for a similar frequency with a honeycomb from the HC sandwich panel : the absorption of the TC specimen is 28% higher than the absorption of the HC specimen.

	Cavities					
	TC					HC
	1	2	3	4	5	1
Measured neck diameter (mm)	2.87 (± 0.02)	1.71 (± 0.01)	1.81 (± 0.02)	2.28 (± 0.02)	2.51 (± 0.02)	1.72 (± 0.02)
Frequency (Hz)	651	798	889	1012	1141	681
Absorption	0.98	0.79	0.86	0.92	1	0.7

Table 5 Maximum absorption of each cavity with the measured dimensions of its hole and its absorption.

The absorption spectrum obtained in this study has not accounted for the full volume of the cavities of the multi-resonator due to the restricted volume available in the impedance tube. With a larger impendence tube, a unit containing the full volume of all cavities could be tested. To reobtain the same absorption spectrum seen in this paper, the diameters of the five necks would require adjustments: in this case, they would need to be wider, according to Equation (1). With a larger impendence tube, more than 5 HR could also be tested.
For the TC acoustic specimens, the frequency range of absorption higher than 90% is about 517 Hz, between 643 Hz and 1160 Hz, which was the main goal of our design.

3.4. Flexural mechanical performance

Two different effects on the 3-point bending mechanical performance of the sandwich panels have been investigated: influence of the design (core wall thickness and core geometry) and influence of a printing parameter (nozzle diameter). Figure 5a shows the schematic of the 3-point bending test: the panel is placed on the two support pins and a force is applied at a constant speed on the sandwich panel through the loading pin until the panel breaks. The 95% confidence intervals are not shown on the graph for clarity purposes. Figure 5b shows the comparison of the average load to displacement ratio in 3-point bending curve before failure for panels TC8×1, HC8×1, TC4×2, HC4×2, TC4×1 and HC4×1. Figure 5c shows the comparison of the highest supported load against the panel weight of TC8×1, HC8×1, TC2×2,

HC4×2, TC4×1 and HC4×1, with their 95% confidence intervals. Table 6 summarizes the stiffness and the highest supported load of each type of panel.

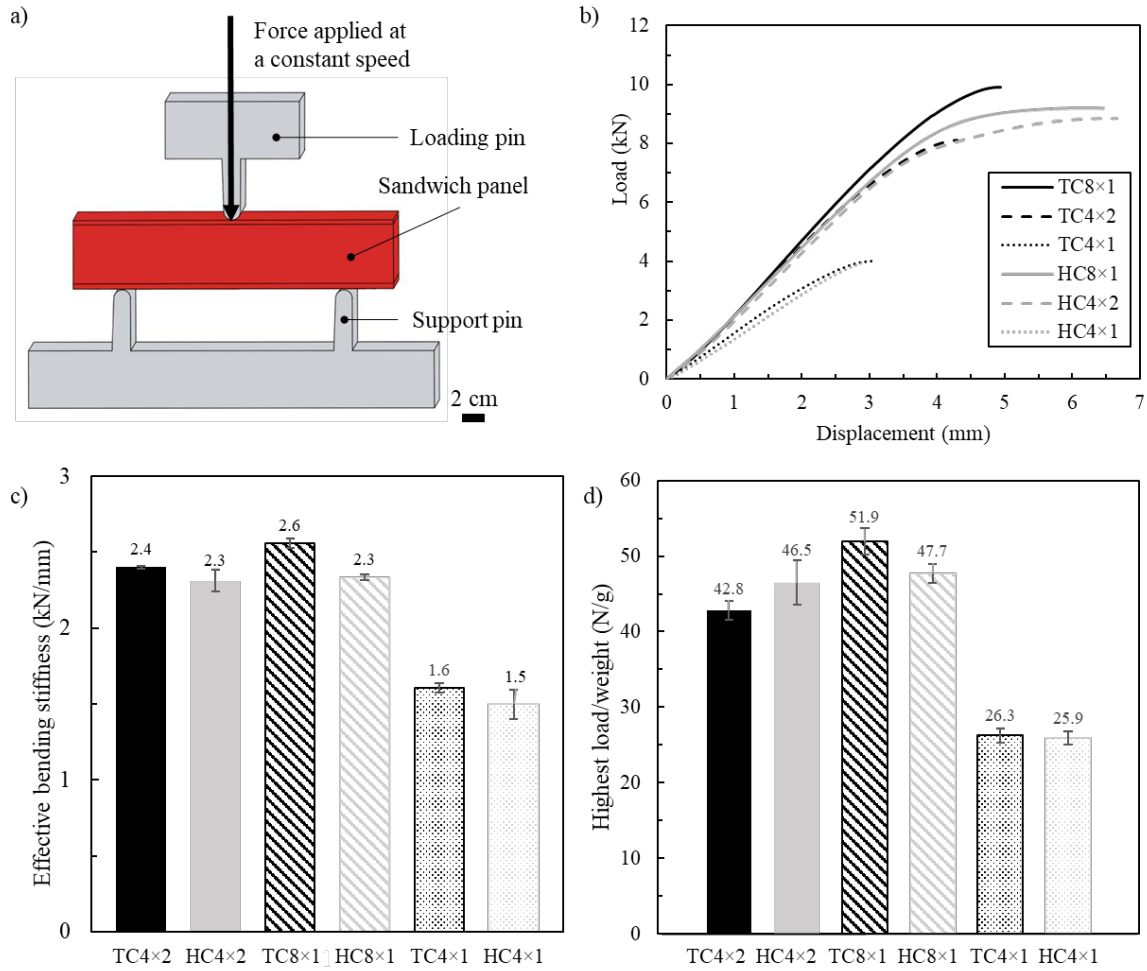

Figure 5 3-point bending test results for the various sandwich panels : a) Schematic of the 3-point bending test setup, b) Average load to displacement ratio curves of panels TC8×1, HC8×1, TC4×2, HC4×2, TC4×1 and HC4×1 in 3-point bending, c) Stiffness of the same panels in 3-point bending: the panel TC8×1 has the highest stiffness, d) Comparison of the average highest supported load to weight ratio of the same panels in 3-point bending: the panel TC8×1 has the highest supported load to weight ratio

Type of panels	Effective bending stiffness (kN/mm)	Max. load (N/g)
TC08×1	2.6 (± 0.1)	51.9 (± 1.7)
TC04×2	2.4 (± 0.1)	42.8 (± 1.2)
TC04×1	1.6 (± 0.1)	26.3 (± 0.9)
HC08×1	2.3 (± 0.1)	47.7 (± 1.2)
HC04×2	2.3 (± 0.1)	46.5 (± 2.9)
HC04×1	1.5 (± 0.1)	25.9 (± 0.9)

Table 6 Average stiffness and highest supported load for each type of sandwich panel

3.4.1. The effect of core geometry: wall thickness

Figure 5c shows that the stiffness values of panels HC8×1 and TC8×1 are respectively 55.3% and 59.0% higher than those measured for panels HC4×1 and TC4×1. The weight of panels HC8×1 and TC8×1 is only ~25% higher than the weight of panels HC4×1 and TC4×1, according to Table 6. Indeed, the skins (~ 108 g in all panels) represent ~56% of panels 8×1 total weight and ~70% in the case of panels 4×1. With the same skins, panels with thinner walls have a lower stiffness than panels with thicker walls. The highest supported load to panel weight ratio is also ~50% higher for panels 8×1 than for panels 4×1.

3.4.2. The effect of core geometry: core shape

Figure 5c shows that when tested under 3-point bending, the stiffness obtained for panels TC8×1, TC4×1 and TC4×2 is higher than that for panels HC8×1, HC4×1 and HC4×2, by respectively 9.9%, 3.9% and 7.3%.

This could be explained by the 2 mm-radius fillets added on all TC panels, which is not the case for the HC panels. Fillets enhance core/skin adhesion by increasing the contact surface between them and therefore reducing debonding between the skin and the core. This increase in stiffness could also be due to the core shape itself since the TC panels, in their core, possess walls perpendicular to the loading pin.

Figure 5d shows that the highest supported load of panel TC8×1 is 8.9% higher than that for panel HC8×1. For the other panels, the highest supported load of panel HC4×2 is 9.2% higher than that of panel TC4×2 and the highest supported load of panel TC4×1 is 1.4% higher than that of panel HC4×1, although in these two cases, it is not significant when taking a 95% confidence interval into account.

We can conclude that the TC geometry cores exhibit a higher stiffness than their HC cores counterparts, and when panels are printed with a nozzle having a diameter of 0.8mm, the

supported load is significantly higher for the TC geometry, in comparison to the HC geometry.

3.4.3. The effect of a printing parameter: nozzles having a diameter of 0.8 mm versus 0.4 mm

The panel TC8×1 has a slightly higher stiffness than that of the panel TC4×2, by 6.7% according to Figure 5c. The difference of stiffness of panels HC8×1 and HC4×2 however is not statistically significant. The maximum supported load is 21.3% higher for panel TC8×1 than for panel TC4×2, but this difference is still not statistically significant for panel HC8×1 and panel HC4×2. The difference of stiffness between the TC specimens could be explained by the inclination of the walls in the core: the contact surface of the filaments might then be better in the case of one large filament rather than two thinner ones, explaining the difference of stiffness and supported load for the TC specimens, a phenomenon not observed for the HC specimens.

The TC8×1 panel exhibits the highest supported load. It is also the fastest panel to print: it takes 33% less time to produce than panel TC4×2 and 42% less time than panel HC8×1. Although a nozzle having a diameter of 0.4 mm would provide more accurate dimensions for the acoustic features, a nozzle having a diameter of 0.8 mm is precise enough to print the holes in the panel skins (the diameter of the holes varies of 0.05 mm in its worst case).

The designed panels are efficient for large broadband sound absorption below 1000 Hz and could be tuned for other frequencies reachable with HR, depending on the applications. The downsides of theses panels, their weight and their consequent time of manufacturing, could be addressed by several improvements. The use of thinner nozzles, such as 0.2 mm, to print thinner walls in the core, and a choice of high temperature reinforced polymers, could increase the mechanical performances of the material used in the panels and compensate the thinning of the walls, while decreasing the panel weight.

4. Conclusion

A wide noise absorption spectrum of ~517 Hz between 643 Hz and 1160 Hz was achieved using a combination of 5 additively manufactured Helmholtz resonators featuring tapered and compact cavities. The acoustic and mechanical performance of 3D-printed TC sandwich panels were compared to a benchmark configuration consisting of a 3D-printed sandwich panel with a standard honeycomb core. The TC panels were better both mechanically and acoustically, when compared to the HC panels. The TC panels were also able to reach a low frequency with a high absorption (651 Hz with 98% of absorption), which was not possible with the HC panel, due to the volume of its cells. The TC panel printed with a nozzle having a diameter of 0.8 mm showed a stiffness higher by ~10% than its benchmark panel with a honeycomb structure of s similar mass.

Further work involving the use of high-performance reinforced thermoplastics (e.g., high temperature-resistant materials) instead of PLA will be undertaken to achieve higher mechanical properties, making this type of acoustic panels interesting for the aerospace industry or any industry requiring the production of acoustic panels with load-bearing capacities. Reducing the fabrication time, as well as decreasing panel weight are also key manufacturing parameters to investigate.

Acknowledgements

The authors acknowledge the technical assistance of Mr. Josué Costa Baptista for the Kundt tube measurements. We also acknowledge the financial support from the FACMO Chair supported by the Natural Sciences and Engineering Research Council of Canada (NSERC, CRDPJ 514761-1), and Safran Group (France).

5. References

[1] European Commission, ed., Flightpath 2050: Europe's vision for aviation ; maintaining global leadership and serving society's needs ; report of the High-Level Group on Aviation Research, Publ. Off. of the Europ. Union, Luxembourg, 2011.

[2] M.J.T. Smith, Aircraft Noise, Cambridge University Press, Cambridge, 1989. https://doi.org/10.1017/CBO9780511584527.

[3] K. Zhao, P. Okolo, E. Neri, P. Chen, J. Kennedy, G.J. Bennett, Noise reduction technologies for aircraft landing gear-A bibliographic review, Progress in Aerospace Sciences. 112 (2020) 100589. https://doi.org/10.1016/j.paerosci.2019.100589.

[4] A. Dubourg, Intégration de structures absorbantes acoustiques innovantes au sein d'une turbosoufflante, masters, École Polytechnique de Montréal, 2015. https://publications.polymtl.ca/2045/ (accessed May 20, 2021).

[5] D. Brzeski, I.L. Hia, J.-F. Chauvette, R.D. Farahani, N. Piccirelli, A. Ross, D. Therriault, Design of thermoset composites for high-speed additive manufacturing of lightweight sound absorbing micro-scaffolds, Additive Manufacturing. 47 (2021) 102245. https://doi.org/10.1016/j.addma.2021.102245.

[6] J. Boulvert, J. Costa-Baptista, T. Cavalieri, M. Perna, E.R. Fotsing, V. Romero-García, G. Gabard, A. Ross, J. Mardjono, J.-P. Groby, Acoustic modeling of micro-lattices obtained by additive manufacturing, Applied Acoustics. 164 (2020) 107244. https://doi.org/10.1016/j.apacoust.2020.107244.

[7] R. Sailesh, L. Yuvaraj, J. Pitchaimani, M. Doddamani, L.B. Mailan Chinnapandi, Acoustic behaviour of 3D printed bio-degradable micro-perforated panels with varying perforation cross-sections, Applied Acoustics. 174 (2021) 107769. https://doi.org/10.1016/j.apacoust.2020.107769.

[8] Z. Liu, J. Zhan, M. Fard, J.L. Davy, Acoustic properties of a porous polycarbonate material produced by additive manufacturing, Materials Letters. 181 (2016) 296–299. https://doi.org/10.1016/j.matlet.2016.06.045.

[9] Frank Fahy, Foundations of Engineering Acoustics, Academic Press, 2001. https://doi.org/10.1016/B978-012247665-5/50005-9.

[10] R. Chanaud, Effects of geometry on the resonance frequency of Helmholtz resonators, Journal of Sound and Vibration. (1994) 337–348. https://doi.org/10.1006/jsvi.1994.1490.

[11] J.G. Lowry, The NASA Acoustically Treated Nacelle Program, The Journal of the Acoustical Society of America. 48 (1970) 780–782. https://doi.org/10.1121/1.1912207.

[12] X. Wei, D. Li, J. Xiong, Fabrication and mechanical behaviors of an all-composite sandwich structure with a hexagon honeycomb core based on the tailor-folding approach, Composites Science and Technology. 184 (2019) 107878. https://doi.org/10.1016/j.compscitech.2019.107878.

[13] Y. Du, N. Yan, M.T. Kortschot, Light-weight honeycomb core sandwich panels containing biofiber-reinforced thermoset polymer composite skins: Fabrication and evaluation, Composites Part B: Engineering. 43 (2012) 2875–2882. https://doi.org/10.1016/j.compositesb.2012.04.052.

[14] X. Peng, J. Ji, Y. Jing, Composite honeycomb metasurface panel for broadband sound absorption, The Journal of the Acoustical Society of America. 144 (2018) EL255–EL261. https://doi.org/10.1121/1.5055847.

[15] M.B. Xu, A. Selamet, H. Kim, Dual Helmholtz resonator, Applied Acoustics. 71 (2010) 822–829. https://doi.org/10.1016/j.apacoust.2010.04.007.

[16] I. Gibson, D. Rosen, B. Stucker, Introduction and Basic Principles, in: I. Gibson, D. Rosen, B. Stucker (Eds.), Additive Manufacturing Technologies: 3D Printing, Rapid

Prototyping, and Direct Digital Manufacturing, Springer, New York, NY, 2015: pp. 1–18. https://doi.org/10.1007/978-1-4939-2113-3_1.
[17] T.S. Srivatsan, T.S. Sudarshan, T.S. Sudarshan, Additive Manufacturing of Materials: Viable Techniques, Metals, Advances, Advantages, and Applications, Additive Manufacturing. (2015). https://doi.org/10.1201/b19360-6.
[18] N. Vidakis, M. Petousis, E. Velidakis, M. Liebscher, V. Mechtcherine, L. Tzounis, On the Strain Rate Sensitivity of Fused Filament Fabrication (FFF) Processed PLA, ABS, PETG, PA6, and PP Thermoplastic Polymers, Polymers. 12 (2020) 2924. https://doi.org/10.3390/polym12122924.
[19] E. García Plaza, P. Núñez López, M. Caminero Torija, J. Chacón Muñoz, Analysis of PLA Geometric Properties Processed by FFF Additive Manufacturing: Effects of Process Parameters and Plate-Extruder Precision Motion, Polymers. 11 (2019) 1581. https://doi.org/10.3390/polym11101581.
[20] D. Pollard, C. Ward, G. Herrmann, J. Etches, The manufacture of honeycomb cores using Fused Deposition Modeling, Advanced Manufacturing: Polymer & Composites Science. 3 (2017) 21–31. https://doi.org/10.1080/20550340.2017.1306337.
[21] M. Mohammadizadeh, I. Fidan, Tensile Performance of 3D-Printed Continuous Fiber-Reinforced Nylon Composites, JMMP. 5 (2021) 68. https://doi.org/10.3390/jmmp5030068.
[22] A. Forés-Garriga, M.A. Pérez, G. Gómez-Gras, G. Reyes-Pozo, Role of infill parameters on the mechanical performance and weight reduction of PEI Ultem processed by FFF, Materials & Design. 193 (2020) 108810. https://doi.org/10.1016/j.matdes.2020.108810.
[23] H. Yazdani Sarvestani, A.H. Akbarzadeh, H. Niknam, K. Hermenean, 3D printed architected polymeric sandwich panels: Energy absorption and structural performance, Composite Structures. 200 (2018) 886–909. https://doi.org/10.1016/j.compstruct.2018.04.002.
[24] A. Redmann, M.C. Montoya-Ospina, R. Karl, N. Rudolph, T.A. Osswald, High-force dynamic mechanical analysis of composite sandwich panels for aerospace structures, Composites Part C: Open Access. 5 (2021) 100136. https://doi.org/10.1016/j.jcomc.2021.100136.
[25] L. Azzouz, Y. Chen, M. Zarrelli, J.M. Pearce, L. Mitchell, G. Ren, M. Grasso, Mechanical properties of 3-D printed truss-like lattice biopolymer non-stochastic structures for sandwich panels with natural fibre composite skins, Composite Structures. 213 (2019) 220–230. https://doi.org/10.1016/j.compstruct.2019.01.103.
[26] A. Bagsik, S. Josupeit, V. Schoeppner, E. Klemp, Mechanical analysis of lightweight constructions manufactured with fused deposition modeling, in: Nuremberg, Germany, 2014: pp. 696–701. https://doi.org/10.1063/1.4873874.
[27] C.R. Liu, J.H. Wu, X. Chen, F. Ma, A thin low-frequency broadband metasurface with multi-order sound absorption, J. Phys. D: Appl. Phys. 52 (2019) 105302. https://doi.org/10.1088/1361-6463/aafaa3.
[28] Y. Tang, F. Li, F. Xin, T.J. Lu, Heterogeneously perforated honeycomb-corrugation hybrid sandwich panel as sound absorber, Materials & Design. 134 (2017) 502–512. https://doi.org/10.1016/j.matdes.2017.09.006.
[29] P. Chesser, B. Post, A. Roschli, C. Carnal, R. Lind, M. Borish, L. Love, Extrusion control for high quality printing on Big Area Additive Manufacturing (BAAM) systems, Additive Manufacturing. 28 (2019) 445–455. https://doi.org/10.1016/j.addma.2019.05.020.
[30] A. Brasington, C. Sacco, J. Halbritter, R. Wehbe, R. Harik, Automated fiber placement: A review of history, current technologies, and future paths forward, Composites Part C: Open Access. 6 (2021) 100182. https://doi.org/10.1016/j.jcomc.2021.100182.

[31] A. Elkaseer, S. Schneider, S.G. Scholz, Experiment-Based Process Modeling and Optimization for High-Quality and Resource-Efficient FFF 3D Printing, Applied Sciences. 10 (2020) 2899. https://doi.org/10.3390/app10082899.
[32] V. Romero-García, G. Theocharis, O. Richoux, V. Pagneux, Use of complex frequency plane to design broadband and sub-wavelength absorbers, The Journal of the Acoustical Society of America. 139 (2016) 3395–3403. https://doi.org/10.1121/1.4950708.